Available online at www.sciencedirect.com

ScienceDirect

International Journal of Heat and Mass Transfer 51 (2008) 3478–3485

International Journal of HEAT and MASS TRANSFER

www.elsevier.com/locate/ijhmt

Optimum length of tubes for heat transfer in turbulent flow at constant wall temperature

Alper Yılmaz *

Department of Mechanical Engineering, University of Çukurova, 01330 Adana, Turkey

Received 14 August 2007
Available online 28 January 2008

Abstract

Maximum heat transfer per cross-sectional area of a tube with smooth wall in turbulent flow at constant wall temperature is determined for a given pressure loss. The dimensionless tube length is determined dependent on the pressure Reynolds number, Prandtl number and inlet local pressure loss coefficient. Limiting cases for short and long tubes are separately investigated. Semi-empirical equations are derived for both optimum dimensionless tube length and dimensionless maximum heat flow per cross-sectional area using numerically obtained values with a maximum deviation of ±6.6% and with a RMSE of 3.5%. The results can also be applied to the channels with non-circular cross-sectional area.

Keywords: Optimum length; Turbulent flow; Constant wall temperature; Forced convection

1. Introduction

Heat exchangers should be constructed as compact as possible. Therefore, they should be designed so that optimum heat transfer occurs. Optimum conditions can occur both for natural and forced convective heat transfer. Different optimum heat transfer conditions are described by Middleman [1].

In many applications heat is transferred by natural convection. Optimum spacing in vertical parallel plates for natural convection is presented by Bar-Cohen and Rohsenow [2] for isothermal symmetric and asymmetric heating and isoflux heating boundary conditions. This problem is investigated numerically by Morrone et al. [3] considering second derivatives in flow direction. Optimum spacing between horizontal cylinders is investigated analytically and numerically by Bejan et al. [4]. Optimum distance between vertical fins by natural convection is determined analytically by Vollaro et al. [5]. Optimum conditions for vertical ducts of arbitrary cross-sectional area are obtained using analytical and experimental results by Yılmaz and Oğulata [6].

Forced convection is the most commonly encountered mode of heat transfer. Bejan and Sciubba [7] and Campo [8] determined optimal plate channel spacing for forced convection. Fowler et al. [9] investigated both numerically and experimentally optimal placing of staggered plates in forced convection. Matos et al. [10] calculated numerically heat transfer around staggered circular and elliptical tubes with constant surface temperature in forced convection. They determined optimal spacing between the circular or elliptical surfaces as a function of Reynolds number. Yılmaz et al. [11] presented optimum dimensions of ducts for laminar flow at constant wall temperature.

In this work, optimum tube length for turbulent flow which allows highest heat transfer per cross-sectional area of the tube with smooth wall is determined. This problem has not been investigated according to the best knowledge of the author.

* Tel.: +90 322 3386772; fax: +90 322 3386126.
E-mail address: alpyil@cu.edu.tr

0017-9310/$ - see front matter © 2007 Elsevier Ltd. All rights reserved.
doi:10.1016/j.ijheatmasstransfer.2007.10.034

Nomenclature

A	cross-sectional area
c_p	specific heat
d	diameter
h	heat transfer coefficient
k	thermal conductivity
L	length of the duct
L^*	dimensionless length, Eq. (19)
Nu	Nusselt number, Eq. (27)
Pr	Prandtl number
$\dot{q}$	heat flux, Eq. (2)
$\dot{q}^*$	dimensionless heat flux, Eq. (9)
$\dot{Q}$	heat flow
p	pressure
Re	Reynolds number, Eq. (15)
Re_p	pressure Reynolds number, Eq. (25)
RMSE	root mean square error
T	temperature
u	velocity
u_p	pressure velocity, Eq. (6)
$\dot{V}$	volume flow rate
x	axial coordinate
z	entrance number, Eq. (28)

Greek symbols

Δp	pressure drop
ΔT	temperature difference, Eq. (5)
ε	porosity
θ	dimensionless temperature, Eq. (7)
λ	pressure loss coefficient
ν	kinematic viscosity
ρ	density

Superscripts and subscripts

*	dimensionless
1	for $\varepsilon = 1$
ε	for $\varepsilon \neq 1$
e	exit
f	frictional
i	inlet, incremental
l	local
m	mean
o	optimum
p	pressure
w	wall

2. Derivation of the equations

Heat transfer in a tube is formulated as

$$\dot{Q} = \rho c_p \dot{V}(T_i - T_e) \tag{1}$$

where $\rho, c_p, \dot{V}, T_i$ and T_e are density, specific heat, volume flow rate, mean inlet and mean exit temperatures of the fluid, respectively. Heat transfer per cross-sectional area is given with the following equation:

$$\dot{q} = \frac{\dot{Q}}{A} = \rho c_p u_m (T_i - T_e) \tag{2}$$

where A and u_m are cross-sectional area and mean fluid velocity, respectively. They are defined as

$$A = \frac{\pi}{4} d^2 \tag{3}$$

$$u_m = \frac{\dot{V}}{A} \tag{4}$$

Using the definitions

$$\Delta T = T_i - T_w \tag{5}$$

$$u_p = \sqrt{2\Delta p/\rho} \tag{6}$$

$$\theta = \frac{T_e - T_w}{\Delta T} \tag{7}$$

$$u^* = \frac{u_m}{u_p} \tag{8}$$

$$q^* = \frac{\dot{q}}{\rho c_p u_p \Delta T} \tag{9}$$

one obtains from Eq. (2)

$$q^* = u^*(1 - \theta) \tag{10}$$

Here, T_w and Δp are constant wall temperature and total pressure loss in the tube, respectively. Total pressure loss consists of frictional pressure loss Δp_f for developed flow, incremental pressure loss Δp_i and local pressure loss Δp_l. Local pressure loss can be calculated by

$$\Delta p_l = \lambda_l \frac{\rho u_m^2}{2} \tag{11}$$

where λ_l is determined from the porosity ε in heat exchangers [11]:

$$\lambda_l = \frac{(3 - \varepsilon)(1 - \varepsilon)^2}{2 - \varepsilon} \tag{12}$$

ε can be envisaged as the ratio of fluid velocities before entering the tube to that in the tube. Frictional pressure loss at developed flow conditions can be calculated from

$$\Delta p_f = \lambda_f \frac{L}{d} \frac{\rho u_m^2}{2} \tag{13}$$

where L is the length of the tube. Frictional pressure loss coefficient λ_f should be calculated with the equation of Prandtl [12],

$$\frac{1}{\lambda_f} = 2.0 \log\left(Re\sqrt{\lambda_f}\right) - 0.80 \tag{14}$$

where Reynolds number Re is defined as

$$Re = \frac{u_m d}{\nu} \tag{15}$$

Here v is kinematic viscosity of the fluid. Incremental pressure loss can be calculated as

$$\Delta p_i = \lambda_i \frac{\rho u_m^2}{2} \tag{16}$$

λ_i values are given by Bhatti and Shah [12]. Using these values, the following equation is derived:

$$\lambda_i = \frac{1}{14.28 + \frac{2}{x^* + 15x^{*5}}} \tag{17}$$

where

$$x^* = \frac{L^*}{Re^{1/4}} \tag{18}$$

Here L^* is defined as

$$L^* = \frac{L}{d} \tag{19}$$

Let us define dimensionless total pressure loss as,

$$\Delta p^* = \frac{\Delta p}{\rho u_m^2/2} \tag{20}$$

where total pressure loss is given by the following formula:

$$\Delta p = \Delta p_f + \Delta p_i + \Delta p_l \tag{21}$$

One can rewrite Eq. (20) as

$$\Delta p^* = \lambda_f \frac{L}{d} + \lambda_i + \lambda_l \tag{22}$$

Introducing Eqs. (6), (8) and (19) in Eq. (22), it follows:

$$u^* = \frac{1}{(\lambda_f L^* + \lambda_i + \lambda_l)^{1/2}} \tag{23}$$

Reynolds number should be calculated from

$$Re = Re_p u^* \tag{24}$$

where pressure Reynolds number Re_p is defined as follows:

$$Re_p = \frac{u_p d}{v} \tag{25}$$

Re_p can also be considered as a dimensionless tube diameter. For given values of Re_p, L^* and λ_l, u^* is determined from Eq. (23) iteratively.

Dimensionless temperature θ in Eq. (10) can be calculated from

$$\theta = \exp(-4Nu\,z) \tag{26}$$

where Nu and z are, respectively, Nusselt number and entrance number and they are defined as follows:

$$Nu = \frac{hd}{k} \tag{27}$$

$$z = \frac{L^*}{RePr} \tag{28}$$

For Nusselt number, one can use the equation proposed by Gnielinski [13]

$$Nu = \frac{\frac{\lambda_f}{8}(Re - 1000)Pr}{1.0 + 12.7(\lambda_f/8)^{1/2}(Pr^{2/3} - 1)}(1 + L^{*-2/3}) \tag{29}$$

For λ_f in this equation, the following equation given by Filonenko [12] should be used

$$\lambda_f = \frac{1}{(1.82 \log Re - 1.64)^2} \tag{30}$$

It is possible to calculate q^* in Eq. (10) with the above equations. This equation is valid for $Pr \geqslant 0.5$, $2300 \leqslant Re \leqslant 10^6$ and $L^* \geqslant 1$. Gnielinski equation is preferred because it has a very wide range of Re and Pr numbers.

3. Equations for long and short tubes

3.1. Long tubes

Local and incremental pressure losses can be neglected for long tubes. In this case, the following equation can be obtained from Eq. (23):

$$u^* = \frac{1}{\sqrt{\lambda_f L^*}} \tag{31}$$

One can use the equation of Blasius [12] for Reynolds number between 10^4 and 10^5:

$$\lambda_f = \frac{0.3164}{Re^{1/4}} \tag{32}$$

Substituting Eqs. (24) and (32) into Eq. (31), the following equation is obtained:

$$u^* = 1.93 Re_p^{1/7} L^{*-4/7} \tag{33}$$

For long tubes, one can assume $\theta \to 0$. Therefore, the equation below is yielded from Eqs. (10) and (33):

$$L^* \to \infty : q^* = 1.93 Re_p^{1/7} L^{*-4/7} \tag{34}$$

3.2. Short tubes

3.2.1. Low Prandtl numbers

For short tubes, one can assume $\theta \to 1$. In this case, Eq. (35) is obtained from Eq. (26):

$$L^* \to 0 : 1 - \theta = 4Nu\,z \tag{35}$$

For Reynolds number between 10^4 and 10^5 and for low Prandtl numbers, one can use the equation of Colburn [12] for Nusselt number with the dependence of L^* in Gnielinski equation (Eq. (29))

$$Nu = 0.023 Re^{0.8} Pr^{1/3}(1 + L^{*-2/3}) \tag{36}$$

Substituting Eqs. (24) and (36) into Eq. (35) yields:

$$1 - \theta = 0.092 Re_p^{-0.8} u^{*-0.2} \frac{L^*}{Pr^{2/3}}(1 + L^{*-2/3}) \tag{37}$$

Using this equation, one obtains from Eq. (10)

$$q^* = 0.092 Re_p^{-0.2} u^{*0.8} \frac{L^*}{Pr^{2/3}}(1 + L^{*-2/3}) \tag{38}$$

Eq. (33) can be used for short tubes in case of $\lambda_l = 0$ also. Substituting Eq. (33) into Eq. (38) yields

$$L^* \to 0 : q^* = 0.1557 \frac{Re_p^{-0.0857}}{Pr^{2/3}} L^{*0.543}(1 + L^{*-2/3}) \tag{39}$$

For short tubes and finite local pressure loss coefficient, it follows from Eq. (23):

$$u^* = \frac{1}{\lambda_l^{1/2}} \tag{40}$$

Substituting Eq. (40) into Eq. (38) yields:

$$L^* \to 0 : q^* = 0.092\lambda_l^{-0.4} \frac{Re_p^{-0.2}}{Pr^{2/3}} L^*(1 + L^{*-2/3}) \tag{41}$$

3.2.2. High Prandtl numbers

The following equation can be used for high Prandtl numbers which is a limiting formulation of Gnielinski equation if Eq. (32) is used for λ_f:

$$Nu = 0.01566 Re^{0.875} Pr^{1/3}(1 + L^{*-2/3}) \tag{42}$$

A very similar equation for high Pr numbers is proposed by Aravinth [14]. If Eq. (42) is used instead of Eq. (36), the equations below can be derived instead of Eqs. (39) and (41), respectively,

$$L^* \to 0 : q^* = 0.1114 L^{*0.5} Pr^{-2/3}(1 + L^{*-2/3}) \tag{43}$$

$$L^* \to 0 : q^* = 0.06264 \lambda_l^{-7/16} Re_p^{-1/8} Pr^{-2/3}(1 + L^{*-2/3}) L^* \tag{44}$$

One can see from the above equations that there are four different equations for short dimensionless tube length L^*.

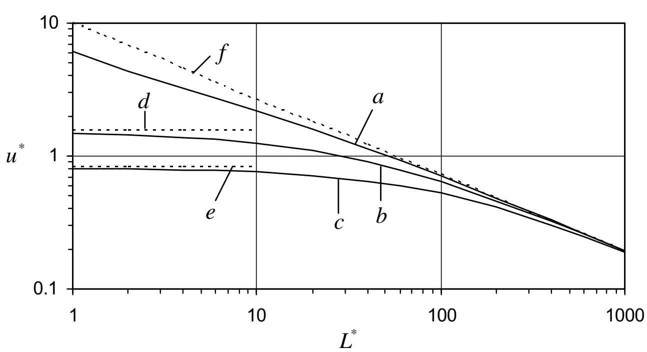

Fig. 1. Variation of dimensionless velocity u^* with dimensionless tube length L^* for $Re_p = 100{,}000$ and for different ε. a: $\varepsilon = 1$; b: $\varepsilon = 0.5$; c: $\varepsilon = 0$; d: (Eq. (40)), $\varepsilon = 0.5$; e: (Eq. (40)), $\varepsilon = 0$; and f: (Eq. (33)).

Table 1
Comparison of numerically calculated $L^*_{o,1}$ values with $L^*_{o,1}$ values obtained from Eq. (45) for various Pr and Re_p numbers ($\varepsilon = 1$)

Re_p	$L^*_{o,1}$ (numerical)	$L^*_{o,1}$ (Eq. (45))	Deviation %
$\varepsilon = 1.0$			
$Pr = 0.7$			
4000	40	41.23	2.993
10,000	59.5	57.71	−3.104
40,000	87.6	86.45	−1.328
100,000	110	104.9	−4.845
400,000	149	140.0	−6.457
1,000,000	178.5	169.5	−5.324
$Pr = 3$			
10,000	115.1	119.5	3.719
40,000	161.4	164.2	1.698
100,000	194	195.9	0.982
400,000	248.3	256.6	3.242
1,000,000	288.3	307.9	6.370
$Pr = 7$			
40,000	250	251.8	0.732
100,000	294.5	295.8	0.445
400,000	368.5	379.6	2.920
1,000,000	421	450.1	6.464
$Pr = 30$			
40,000	573.5	576.5	0.522
100,000	667	663.7	−0.492
400,000	813	824.4	1.385
1,000,000	916	954.9	4.074
$Pr = 70$			
40,000	946	962.0	1.662
100,000	1105	1102.3	−0.247
400,000	1341	1356.7	1.158
1,000,000	1500	1559.1	3.793

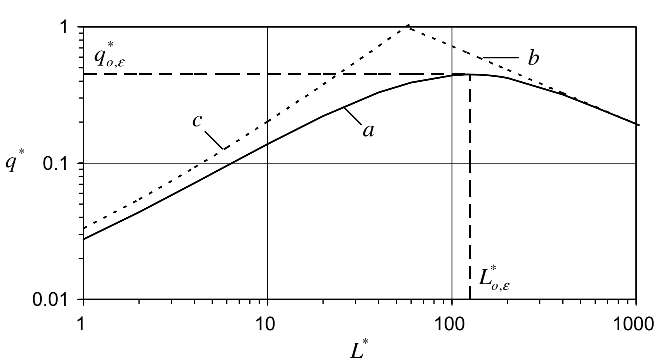

Fig. 2. Variation of dimensionless heat flux q^* with dimensionless tube length L^* for $\varepsilon = 0.5$, $Pr = 0.7$ and $Re_p = 100{,}000$ (curve a). b: Eq. (34); c: Eq. (41).

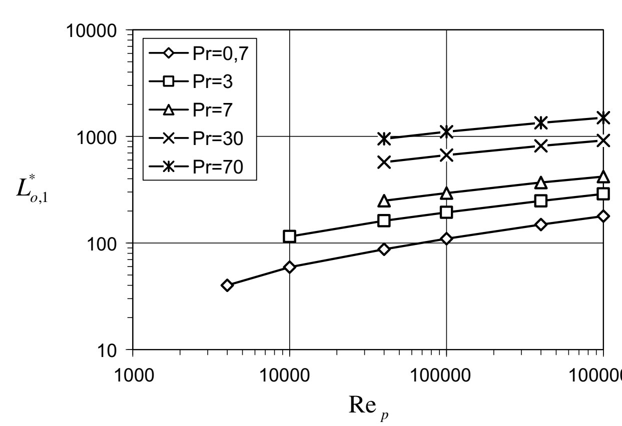

Fig. 3. Variation of optimum dimensionless tube length $L^*_{o,1}$ ($\varepsilon = 1$) with Re_p for different Pr numbers.

4. Results

In Fig. 1, dimensionless velocity u^* is shown as a function of L^* for different ε values with a given Re_p value. u^* decreases with increasing L^* because of the increase in frictional pressure loss. Without any local pressure loss ($\varepsilon = 1$), u^* increases steadily with decreasing L^* values.

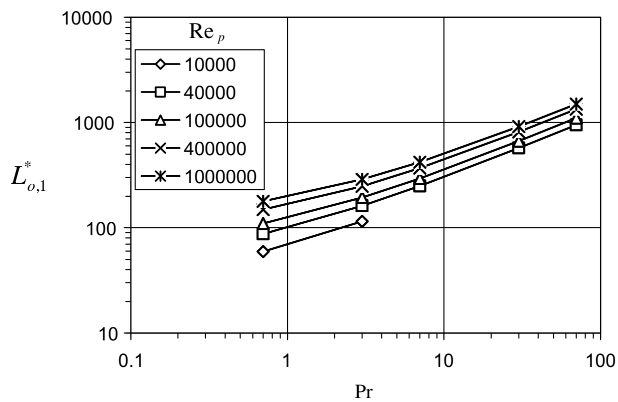

Fig. 4. Variation of optimum dimensionless tube length $L^*_{o,1}(\varepsilon = 1)$ with Pr for different Re_p numbers.

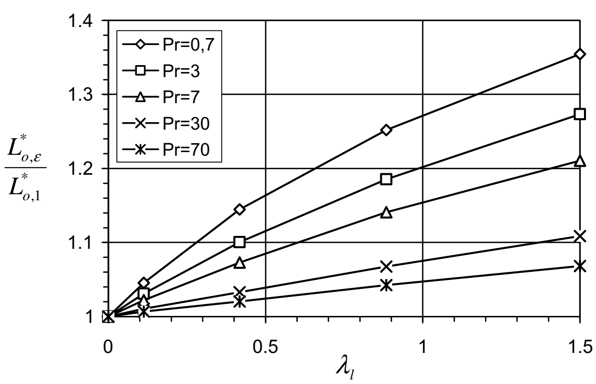

Fig. 5. Variation of $L^*_{o,\varepsilon}/L^*_{o,1}$ with λ_l for different Pr numbers ($Re_p = 100{,}000$).

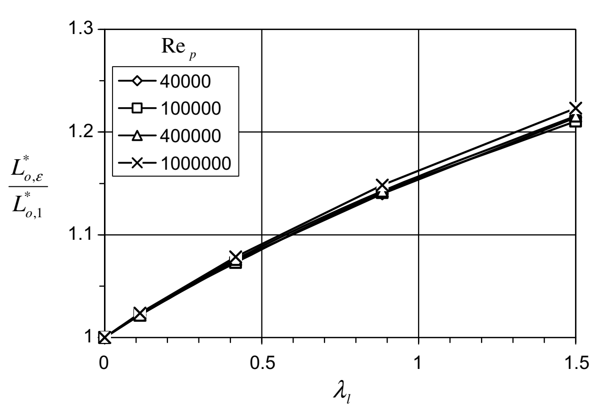

Fig. 6. Variation of $L^*_{o,\varepsilon}/L^*_{o,1}$ with λ_l for different Re_p numbers ($Pr = 7$).

Curves a, b and c are valid for $\varepsilon = 1$, $\varepsilon = 0.5$ and $\varepsilon = 0$, respectively. Curves d and e are limiting curves for $L^* \to 0$

Table 2
Comparison of numerically calculated $L^*_{o,\varepsilon}$ values with $L^*_{o,\varepsilon}$ values obtained from Eq. (46) for various Pr and Re_p numbers at different ε's

Re_p	$L^*_{o,\varepsilon}$ (numerical)	$L^*_{o,\varepsilon}$ (Eq. (46))	Deviation %
$\varepsilon = 0$			
$Pr = 0.7$			
10,000	85.5	80.98	−5.584
40,000	119	121.3	1.906
100,000	149	147.2	−1.207
400,000	203	196.4	−3.361
1,000,000	243.5	237.8	−2.390
$Pr = 3$			
40,000	207	210.9	1.862
100,000	247	251.7	1.866
400,000	318	329.7	3.540
1,000,000	370.5	395.6	6.337
$Pr = 7$			
40,000	303.5	306.048	0.8326
100,000	356.5	359.4864	0.8307
400,000	448	461.2846	2.880
1,000,000	515	546.9702	5.845
$Pr = 30$			
40,000	638	636.5	−0.2392
100,000	739.5	732.8	−0.9180
400,000	906	910.2	0.4576
1,000,000	1026	1054.2	2.678
$Pr = 70$			
40,000	1014.5	1023.7	0.8968
100,000	1180.5	1173.0	−0.6416
400,000	1437	1443.7	0.4657
1,000,000	1615	1659.1	2.660
$\varepsilon = 0.50$			
$Pr = 0.7$			
10,000	70.1	66.07	−6.107
40,000	100.7	98.97	−1.747
100,000	125.9	120.11	−4.821
400,000	170.9	160.2	−6.659
1,000,000	204.9	194.0	−5.608
$Pr = 3$			
10,000	130	131.8	1.341
40,000	178.5	181.0	1.367
100,000	213.5	216.0	1.136
400,000	274.5	282.9	2.953
1,000,000	319	339.4	6.009
$Pr = 7$			
40,000	268.8	271.3	0.9246
100,000	316	318.7	0.8413
400,000	396.5	408.9	3.038
1,000,000	454	484.9	6.369
$Pr = 30$			
40,000	594	598.0	0.6766
100,000	689	688.5	−0.0686
400,000	843	855.2	1.428
1,000,000	951	990.6	3.995
$Pr = 70$			
40,000	966.5	984.1	1.792
100,000	1127.5	1127.7	0.0148
400,000	1370	1388.0	1.294
1,000,000	1538	1595.0	3.577

and they are calculated according to Eq. (40) for $\varepsilon = 0.5$ and $\varepsilon = 0$, respectively. Curve f is a limiting curve for $L^* \to \infty$ and it is calculated according to Eq. (33).

In Fig. 2, q^* is illustrated dependent on L^* as curve a. One can see clearly from this figure that, q^* has a maximum value at a certain dimensionless length L^*. Optimum dimensionless heat flux and tube length are respectively designated as $q^*_{o,\varepsilon}$ and $L^*_{o,\varepsilon}$ for $\varepsilon = 0.5$. Limiting curve b is calculated according to Eq. (34) for $L^* \to \infty$. Limiting curve c for $L^* \to 0$ is calculated using Eq. (41) for $\varepsilon = 0.5$.

The values for L^*_o are given in Table 1 for different Pr and Re_p values for $\varepsilon = 1 (L^*_{o,1})$. $L^*_{o,1}$ values are presented in Figs. 3 and 4 as a function of Re_p and Pr numbers, respectively. In these figures, some points for low Re_p and high Pr numbers are not calculated because laminar flow prevails in these cases. Dependency of $L^*_{o,1}$ on Re_p is slightly stronger at lower Re_p numbers as can be seen from Fig. 3. In contrast, dependency of $L^*_{o,1}$ on Pr number is slightly stronger at high values of Pr number as demonstrated in Fig. 4.

The following equation is derived from the numerically obtained values of $L^*_{o,1}$:

$$L^*_{o,1} = 14.73 Re_p^{0.145} Pr^{0.62} \left(1 + \frac{0.174 Re_p^{1/3} Pr^{-1.15}}{(1 + 5.810^{10} Re_p^{-8/3})}\right)^{0.2} \quad (45)$$

The values calculated using this equation is given in Table 1, also. This equation describes the real optimum values with $\pm 6.5\%$ maximum error and 3.4% RMSE which can be considered as a good approximation.

Eq. (45) is valid for $\varepsilon = 1$ $(\lambda_1 = 0)$. For other ε values, one designates L^*_o as $L^*_{o,\varepsilon}$. The values for the ratio $L^*_{o,\varepsilon}/L^*_{o,1}$ are given in Figs. 5 and 6 as a function of λ_1 for different values of the parameters Pr and Re_p, respectively. The influence of λ_1 on the ratio $L^*_{o,\varepsilon}/L^*_{o,1}$ can be neglected at high values of Pr number as demonstrated in Fig. 5. As can be seen from Fig. 6, effect of Re_p on $L^*_{o,\varepsilon}/L^*_{o,1}$ is negligible. Therefore, $L^*_{o,\varepsilon}$ can be described with the following equation:

$$L^*_{o,\varepsilon} = L^*_{o,1}\left[1 + \frac{0.27 Pr^{-0.22}\lambda^{0.8}}{(1 + 0.02 Pr^2)^{0.18}}\right] \quad (46)$$

In Table 2, values of $L^*_{o,\varepsilon}$ calculated numerically and determined according to Eq. (46) are given for different Re_p, Pr and ε. As can be seen from the table, Eq. (46) describes the real optimum values with $\pm 6.6\%$ maximum error with a RMSE of 3.5.

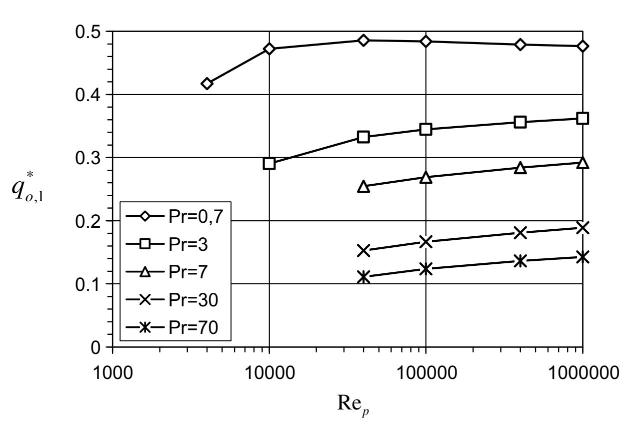

Fig. 7. Variation of optimum dimensionless heat flux $q^*_{o,1} (\varepsilon = 1)$ with Re_p for different Pr numbers.

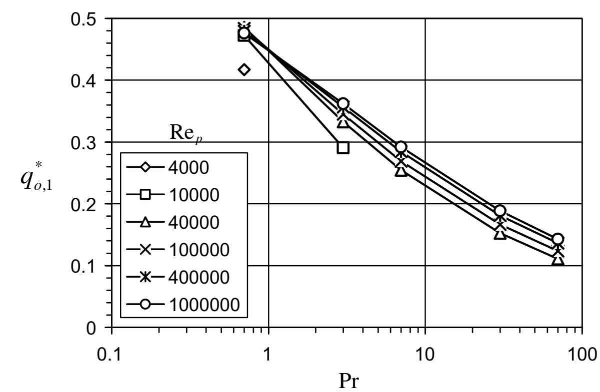

Fig. 8. Variation of optimum dimensionless heat flux $q^*_{o,1} (\varepsilon = 1)$ with Pr for different Re_p numbers.

Table 3
Comparison of numerically calculated $q^*_{o,1}$ values with $q^*_{o,1}$ values obtained from Eq. (47) for various Pr and Re_p numbers ($\varepsilon = 1$)

Re_p	$q^*_{o,1}$ (numerical)	$q^*_{o,1}$ (Eq. (47))	Deviation %
$\varepsilon = 1.0$			
$Pr = 0.7$			
4000	0.4170	0.4389	4.991
10,000	0.4724	0.4577	−3.215
40,000	0.4855	0.4758	−2.031
100,000	0.4838	0.4820	−0.3752
400,000	0.4791	0.4863	1.483
1,000,000	0.4763	0.4875	2.306
$Pr = 3$			
10,000	0.2905	0.2926	0.6963
40,000	0.3327	0.3204	−3.829
100,000	0.3449	0.3361	−2.627
400,000	0.3562	0.3525	−1.069
1,000,000	0.3619	0.3585	−0.9560
$Pr = 7$			
40,000	0.2545	0.2434	−4.579
100,000	0.269	0.2594	−3.723
400,000	0.2841	0.281	−1.106
1,000,000	0.2919	0.2918	−0.040
$Pr = 30$			
40,000	0.1526	0.1475	−3.469
100,000	0.1667	0.1586	−5.118
400,000	0.181	0.1763	−2.627
1,000,000	0.1888	0.1884	−0.2211
$Pr = 70$			
40,000	0.1109	0.1098	−1.063
100,000	0.1238	0.1181	−4.837
400,000	0.1363	0.1317	−3.441
1,000,000	0.1429	0.1414	−0.9973

Optimum dimensionless heat flux q_o^* for $\varepsilon = 1(q_{o,1}^*)$ is shown in Figs. 7 and 8 as a function of Re_p and Pr numbers, respectively. Similar to Figs. 3 and 4, some points are not calculated due to the transition to laminar flow. One can see from these figures that the dependency of $q_{o,1}^*$ on Re_p is very weak compared to the dependency on Pr number. The following equation is derived for $q_{o,1}^*$:

$$q_{o,1}^* = \frac{0.455}{Pr^{0.2}(1 + 2500 Pr^{1.5} Re_p^{-0.8})^{0.1}} \tag{47}$$

The values calculated using this equation is compared in Table 3 with the numerically obtained values. Eq. (47) describes real values with a maximum error of ±5% and RMSE of 2.9%.

q_o^* values for $\varepsilon \neq 1$ is designated as $q_{o,\varepsilon}^*$. In Figs. 9 and 10, the ratio $q_{o,1}^*/q_{o,\varepsilon}^*$ is given as a function of λ_l for different Pr and Re_p values, respectively. With increasing Pr number, the influence of local loss coefficient λ_l decreases as demonstrated in Fig. 9. As can be seen from Fig 10, the dependency of $q_{o,1}^*/q_{o,\varepsilon}^*$ on Re_p number can be neglected. The following equation is derived for $q_{o,\varepsilon}^*$:

$$q_{o,\varepsilon}^* = \frac{q_{o,1}^*}{1 + \frac{0.155 Pr^{-0.34} \lambda_l^{0.88}}{(1 + 0.0385 Pr^{1.48})^{0.25}}} \tag{48}$$

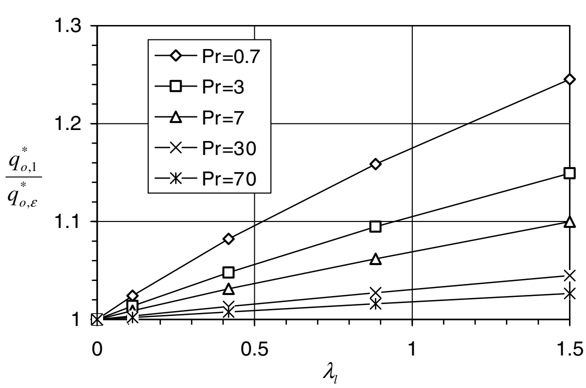

Fig. 9. Variation of $q_{o,1}^*/q_{o,\varepsilon}^*$ with λ_l for different Pr numbers ($Re_p = 100{,}000$).

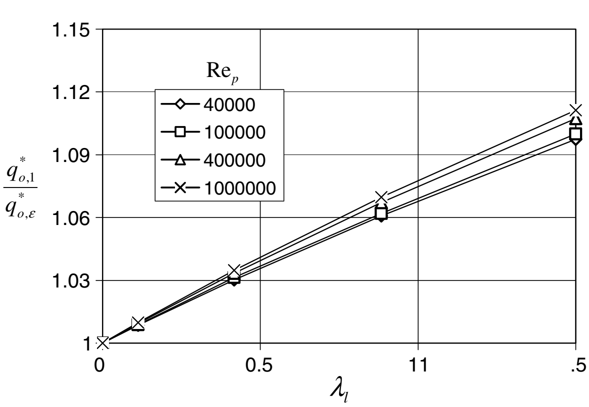

Fig. 10. Variation of $q_{o,1}^*/q_{o,\varepsilon}^*$ with λ_l for different Re_p numbers ($Pr = 7$).

The values calculated according to this equation is compared with the real values determined numerically in Table 4.

Table 4
Comparison of numerically calculated $q_{o,\varepsilon}^*$ values with $q_{o,\varepsilon}^*$ values obtained from Eq. (48) for various Pr and Re_p numbers at different ε's

Re_p	$q_{o,\varepsilon}^*$ (numerical)	$q_{o,\varepsilon}^*$ (Eq. (48))	Deviation %
$\varepsilon = 0$			
$Pr = 0.7$			
10,000	0.3726	0.3666	−1.647
40,000	0.3883	0.3811	−1.906
100,000	0.3886	0.3860	−0.651
400,000	0.3863	0.3895	0.8133
1,000,000	0.3848	0.3905	1.453
$Pr = 3$			
40,000	0.2905	0.2797	−3.863
100,000	0.3001	0.2933	−2.313
400,000	0.3087	0.3076	−0.3411
1,000,000	0.3128	0.3129	0.0373
$Pr = 7$			
40,000	0.2320	0.2212	−4.860
100,000	0.2446	0.2357	−3.763
400,000	0.2566	0.2554	−0.4670
1,000,000	0.2627	0.2652	0.9527
$Pr = 30$			
40,000	0.1463	0.1415	−3.462
100,000	0.1595	0.1520	−4.925
400,000	0.1724	0.1691	−2.003
1,000,000	0.1794	0.1806	0.6987
$Pr = 70$			
40,000	0.1081	0.1072	−0.9055
100,000	0.1206	0.1153	−4.598
400,000	0.1324	0.1286	−2.912
1,000,000	0.1385	0.1381	−0.2699
$\varepsilon = 0.50$			
$Pr = 0.7$			
10,000	0.4330	0.4236	−2.219
40,000	0.4478	0.4403	−1.685
100,000	0.4470	0.4461	−0.2122
400,000	0.4435	0.4501	1.469
1,000,000	0.4412	0.4512	2.211
$Pr = 3$			
10,000	0.2765	0.2794	1.044
40,000	0.3181	0.306	−3.957
100,000	0.3291	0.3209	−2.562
400,000	0.3394	0.3365	−0.8504
1,000,000	0.3445	0.3423	−0.6373
$Pr = 7$			
40,000	0.2471	0.2357	−4.815
100,000	0.2609	0.2512	−3.843
400,000	0.2749	0.2722	−1.016
1,000,000	0.2821	0.2826	0.1756
$Pr = 30$			
40,000	0.1507	0.1455	−3.598
100,000	0.1645	0.1564	−5.195
400,000	0.1784	0.1739	−2.561
1,000,000	0.1859	0.1858	−0.0509
$Pr = 70$			
40,000	0.1101	0.1089	−1.103
100,000	0.1228	0.1172	−4.857
400,000	0.1351	0.1307	−3.373
1,000,000	0.1416	0.1403	−0.8704

Eq. (47) describes real numerically obtained values with a maximum deviation of ±5.1% and RMSE of 2.4%.

L_o^* and q_o^* values can be determined from Eqs. (45)–(48). Reynolds number should be calculated using Eq. (24) to see whether the flow is turbulent or not. u^* values in this equation can be approximately calculated from the equation below:

$$u^* = \frac{1}{(\lambda_l + 0.2685 L^{*8/7} Re_p^{-2/7})^{1/2}} \tag{49}$$

Using this approximate value, u^* can be exactly determined from Eq. (23) iteratively.

5. Conclusions

It is shown that a certain tube length to diameter ratio (L^*) in turbulent tube flow exists which results in maximum heat transfer per tube cross-sectional area. This value is dependent on pressure Reynolds number Re_p, Prandtl number Pr and local pressure loss coefficient λ_l.

Optimum value of L^* increases with Pr and Re_p numbers. Local pressure loss coefficient of the tube λ_l has an influence on optimum value of L^* only at low Pr numbers. For Pr values higher than 30, the influence of λ_l can be neglected.

Maximum heat transfer per cross-sectional area increases with Re_p and decreases with Pr number. Maximum heat transfer per cross-sectional area decreases with local pressure loss coefficient; however, this can be neglected for $Pr > 30$.

References

[1] S. Middleman, An Introduction to Mass and Heat Transfer, Principles of Analysis and Design, John Wiley and Sons, New York, 1998 (Chapter 12).

[2] A. Bar-Cohen, W.M. Rohsenow, Thermally optimum spacing of vertical natural convection cooled parallel plates, J. Heat Transfer (106) (1984) 116–123.

[3] B. Morrone, A. Campo, O. Manca, Optimum plate separation in vertical parallel-plate channels for natural convective flows: incorporation of large spaces at the channel extremes, Int. J. Heat Mass Transfer (40) (1997) 993–1000.

[4] A. Bejan, A.J. Fowler, G. Stanescu, The optimal spacing between horizontal cylinders in a fixed volume cooled by natural convection, Int. J. Heat Mass Transfer (38) (1995) 2047–2055.

[5] A. Vollaro, S. Grignaffini, F. Gugliermetti, Optimum design of vertical rectangular fin arrays, Int. J. Therm. Sci. (38) (1999) 525–529.

[6] T. Yılmaz, R.T. Oğulata, Natural convection heat transfer in vertical channels of arbitrary cross-sections, in: T.N. Veziroğlu (Ed.), Heat and Mass Transfer: An Era of Change, Nova Science, New York, 1993, pp. 181–201.

[7] A. Bejan, E. Sciubba, The optimal spacing of parallel plates cooled by forced convection, Int. J. Heat Mass Transfer (35) (1992) 3259–3264.

[8] A. Campo, Bounds for the optimal conditions of forced convective flows inside multiple channels whose plates are heated by a uniform flux, Int. Commun. Heat Mass Transfer (26) (1999) 105–114.

[9] A.J. Fowler, G.A. Ledezma, A. Bejan, Optimal geometric arrangement of staggered plates in forced convection, Int. J. Heat Mass Transfer (40) (1997) 1795–1805.

[10] R.S. Matos, J.V.C. Vargas, T.A. Laursen, F.E.M. Saboya, Optimization study and heat transfer comparison of staggered circular and elliptic tubes in forced convection, Int. J. Heat Mass Transfer (44) (2001) 3953–3961.

[11] A. Yılmaz, O. Büyükalaca, T. Yılmaz, Optimum shape and dimensions of ducts for convective heat transfer in laminar flow at constant wall temperature, Int. J. Heat Mass Transfer (43) (2000) 767–775.

[12] M.S. Bhatti, R.K. Shah, Turbulent flow and transition flow convective heat transfer in ducts, in: S. Kakaç, R.K. Shah, W. Aung (Eds.), Handbook of Single-Phase Convective Heat Transfer, John Wiley and Sons, New York, 1987, pp. 4.24–4.43.

[13] V. Gnielinski, New equations for heat and mass transfer in turbulent pipe and channel flow, Int. Chem. Eng. (16) (1976) 359–368.

[14] S. Aravinth, Prediction of heat and mass transfer for fully developed turbulent fluid flow through tubes, Int. J. Heat Mass Transfer (43) (2000) 1399–1408.